

Characterizing Quantum Coherence via Schur–Horn Majorization: Degenerate Distillation and Refined Entropic Uncertainty

Tariq Aziz¹, Meng-Long Song¹, Liu Ye¹, Dong Wang^{1,*}

¹*School of Physics and Optoelectronic Engineering, Anhui University, Hefei 230601, China*

*Email: dwang@ahu.edu.cn

1. Abstract:

We develop a rigorous framework for quantifying quantum coherence in finite-dimensional systems by applying the Schur–Horn majorization theorem to relate eigenvalue distributions and diagonal entries of density matrices. Building on this foundation, we introduce a versatile suite of coherence measures—including the relative cross-entropy of coherence and its partial variants—that satisfy all resource-theoretic axioms under incoherent operations. This unifying approach clarifies the geometric boundaries of physically realizable states in von Neumann–Tsallis entropy space and uncovers the phenomenon of degenerate coherence distillation, where symmetry in the eigenvalue spectrum enables enhanced coherence extraction in higher-dimensional systems. In addition, we strengthen entropy-based uncertainty relations by refining the Massen–Uffink bound to account for the largest eigenvalues across distinct measurement bases. This refinement forges a deeper connection between entropy and uncertainty, which yields operationally meaningful constraints for quantum information tasks. Altogether, our findings illustrate the power of majorization in resource-theoretic analyses of quantum coherence, which offer valuable tools for both fundamental research and real-world applications in quantum information processing.

2. Introduction:

Coherence, a fundamental phenomenon in quantum optics and polarization theory, has long been associated with two-point correlation functions that quantify the interference capability of a wave field [1-3]. From the perspective of resource theory, however, coherence is contextual, which means that it is

treated as a physical resource that depends on the off-diagonal elements of the density matrix relative to a preferred basis [4-5]. This viewpoint introduces a quantitative framework to assess coherence and its transformations under quantum operations. In this framework, free operations are central to the resource theory of quantum coherence, defined as quantum operations that map the set of incoherent states onto itself. The incoherent operation (IO) ensures no coherence is generated from an incoherent state under any measurement outcome, even probabilistically [4]. A stricter subset of IOs, known as Strictly Incoherent Operations (SIO), imposes the additional constraint that prevents the generation or detection of coherence in the context that both Kraus operators and their duals preserve the set of incoherent states [6-8]. Maximally Incoherent Operations (MIO), on the other hand, represent the broadest class, which map incoherent states into themselves, but without the stricter restrictions on individual quantum operators [6-8]. This hierarchy of operations—MIO, IO, and SIO—establishes the framework for resource-theoretic coherence, with implications for quantum measurement, transformations, and entropy dynamics under these operations [8]. These frameworks lay the foundation for developing coherence monotones and measures, crucial for quantifying and analyzing coherence in quantum systems.

Coherence monotones and measures are essential for understanding and quantifying quantum coherence, particularly under different classes of free operations (IO and SIO) [8]. In resource theory, coherence quantifiers should satisfy certain postulates, including faithfulness, monotonicity, strong monotonicity under selective IO, and convexity [4]. Key measures include the relative entropy of coherence, $C_r(\rho) = S(\Delta[\rho]) - S(\rho)$, which represents the information-theoretic deviation of a state from its decohered $\Delta[\rho]$ counterpart. This measure is operationally significant, being linked to coherence distillation and monotonicity under IO [4]. Another measure, the l_1 -norm of coherence, $C_{l_1}(\rho) = \sum_{i,j} |\rho_{ij}| - 1$, directly captures the magnitude of off-diagonal elements in the density matrix ρ and provides an intuitive quantification of coherence [4,8]. These measures have distinct properties: while $C_r(\rho)$ connects coherence with thermodynamic tasks and entanglement, $C_{l_1}(\rho)$ is computationally

simpler and highlights the role of matrix norms. Under stricter operations like SIO, coherence monotonicity is preserved where no coherence is generated in any measurement outcome, which emphasizes robustness in theoretical and experimental applications.

Based on the foundational role of coherence quantification in resource theories, Du et al. [9] attempted to characterize coherence transformations under IO by using the majorization criterion, where they asserted that a pure state $|\varphi\rangle$ can be transformed into $|\psi\rangle$ if and only if $\Delta[|\psi\rangle\langle\psi|] > \Delta[|\varphi\rangle\langle\varphi|]$. However, these results have incomplete proof, particularly for higher-dimensional systems. Chitambar et al. [6-7] addressed these gaps by refining the definition of IO and introducing SIO, which ensured that both Kraus operators and their duals preserve the set of incoherent states. This refinement emphasized the need for operational rigor in coherence theories. Zhu et al. [10] rigorously proved the majorization criterion for IO and SIO and demonstrated that the coherence monotones under these operations follow the same structural properties as entanglement monotones. They showed that coherence monotones, defined using real symmetric concave functions f over the probability simplex \mathcal{F}_{sc} , follow the same structural properties as entanglement monotones. For pure states $|\psi\rangle$, the coherence monotone is given by $C_f(|\psi\rangle) = f(\mu(|\psi\rangle))$, where $\mu(|\psi\rangle)$ represents the vector of eigenvalues in descending order, while for mixed states, coherence monotones generalize to $C_f(\rho) = \min_{\{p_j, \rho_j\}} \sum_j p_j C_f(\rho_j)$, where the minimization is taken over all pure state decompositions of $\rho = \sum_j p_j \rho_j$. This concave and symmetric construction reinforces the monotonicity and convexity of coherence measures under IO and SIO, thereby it solidifies the theoretical framework of coherence as a resource.

On the other hand, the relationships between entropy, the index of coincidence, and error probability were examined in Refs. [11-12] where the authors presented analytical bounds and geometric representation with applications in cryptography and rate-distortion theory. A. Aiello and J.P. Woerdman [13] further explored the constraints on polarization entropy and depolarization indices in light scattering, in which they defined universal boundaries in the entropy-depolarization plane. Tariq et.al. [14]

introduced a geometric framework using the purity-index–depolarization-index plane to describe the scattering properties of polarized light scattering and recovered entropy-depolarization plane via indices of purity. The approach simplifies light scattering analysis, which may offer practical applications in biomedical imaging and radar polarimetry by providing a clear classification of depolarization properties without computational complexity. More recently, some authors [15-16] utilized information diagrams to derive tighter bounds for entropy uncertainty relation (EUR). These results are applied to quantum measurements, including mutually unbiased bases and SIC-POVMs, which may offer improved methods to detect non-classical correlations such as entanglement and steerability. Together, these studies highlight the versatility of entropy in analyzing uncertainty, randomness, and structural properties across classical and quantum information science and optics. However, due to the indescribable boundary curves, the improvement on lowering estimates on the Shannon entropy was only approximated by the smooth curves with suitable polygonal lines [15], where this issue is resolved in our approach.

In this work, we employ the Schur–Horn (SH) majorization theorem to construct fundamental coherence measures, including the relative cross-entropy of coherence and its partial variants. By utilizing the majorization relationship between the eigenvalues of density matrices and their diagonal entries, these measures form a robust framework for coherence quantification. A central aspect of our study is the characterization of entropy–coherence monotones derived from SH majorization, which we visualize within von Neumann–Tsallis entropy diagram. This approach enables an efficient and precise delineation of physically realizable regions for any d -dimensional quantum state. In particular, by analytically mapping boundary curves and subspaces tied to specific eigenvalue distributions, we overcome a longstanding challenge in information-diagram methods—namely, the lack of exact boundary descriptions [15].

Furthermore, we propose an operational entropy uncertainty relation that refines the Massen–Uffink bound by substituting the overlap of maximal eigenstates in the X and Z bases with the sum of their largest eigenvalues. This refinement establishes a deeper link between entropy and uncertainty, which

yields operationally meaningful constraints with direct applications in quantum information tasks. In the following sections, we detail how these results not only enhance our theoretical understanding of coherence as a quantum resource but also provide practical tools for a variety of quantum technologies.

3. The Suhr-Horn Majorization and coherence monotones:

The mathematical foundation of coherence measures like relative entropy of coherence is deeply connected to the SH majorization theorem which is associated with the symplectic geometry through the Atiyah-Guillemin-Sternberg (AGS) convexity theorem, which asserts that the image of a compact connected symplectic manifold under a moment map is a convex polytope [17-18]. This result has profound implications in quantum mechanics, as it connects the symplectic structure of Hermitian matrices to convex geometric objects, which may allow us to describe the eigenvalues distribution of quantum states geometrically. The moment map associates a Hermitian matrix $A \in \mathcal{H}(d)$ to its diagonal matrix under the action of the maximal torus $T \subset U(d)$ captures the relationship between its spectral and diagonal components. The coadjoint orbits in the unitary Lie group $U(d)$ play a central role in this framework. For a Hermitian matrix or more specifically a d – dimensional density matrix ρ with eigenvalue vector λ where $\lambda_1 \geq \lambda_2 \geq \dots \geq \lambda_d$, the coadjoint orbit \mathcal{O}_λ of ρ under the action of $U(d)$ consists of all matrices unitarily equivalent to ρ . The projection of its orbit onto the diagonal matrices, via the moment map, forms a convex polytope. This projection is governed by majorization relations, which establishes a direct link to the SH theorem. Specifically, the convex polytope formed by the diagonals of matrices in $\mathcal{O}_{\rho_{ii}}$ is characterized by a condition $\rho_{ii} \preceq \lambda$, where ρ_{ii} is the vector of diagonal elements of a density matrix $\rho_{11} \geq \rho_{22} \geq \dots \geq \rho_{dd}$, which means that,

$$\sum_{i=1}^k \lambda_i^\downarrow \geq \sum_{i=1}^k \rho_{ii}^\downarrow, \quad \forall k, \quad (01)$$

where symbol \downarrow represents the descending order, with equality for $k = d$. The matrix of diagonal elements ρ_{diag} with zero off-diagonal elements is majorized by ρ , which means that $\rho_{diag} =$

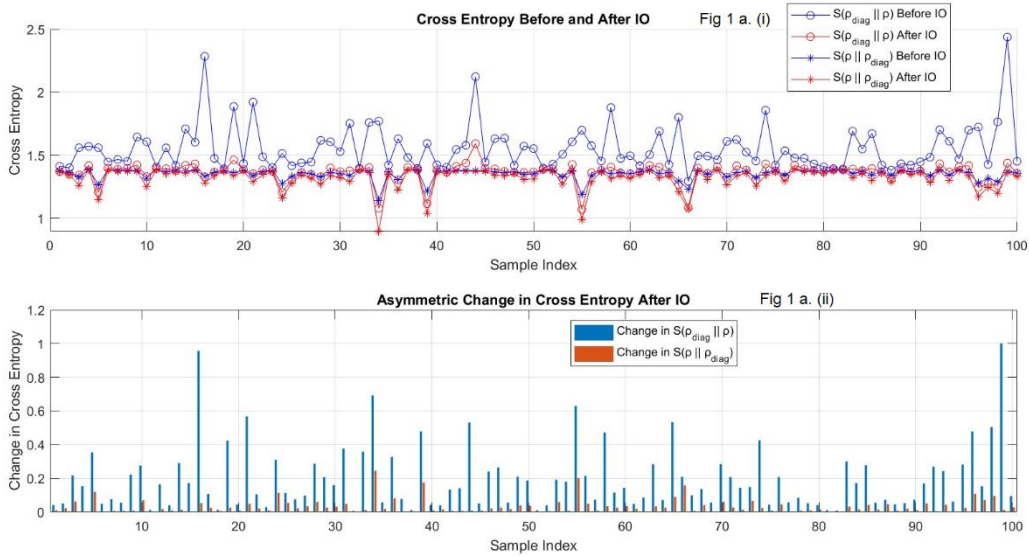
$\sum_j p_j U_j \rho U_j^\dagger$, where U_j are unitary operators $\{p_j\}$ are probabilities. By the concavity of the von Neumann entropy of decohered state $S(\rho_{diag})$, i.e., $S(\sum_j p_j \rho_{diag_j}) \geq \sum_j p_j S(\rho_{diag_j})$ [19], we have $S(\rho_{diag}) \geq \sum_j p_j S(U_j \rho U_j^\dagger) = \sum_j p_j S(\rho) = S(\rho)$, as it is invariant under unitary transformation and the probabilities sum to 1 ($\sum_j p_j = 1$). Hence, $S(\rho_{diag}) \geq S(\rho) \Rightarrow C_r(\rho) = S(\rho_{diag}) - S(\rho) \geq 0$, which is the relative entropy of coherence [4]. The same result can be derived by taking the negative logarithm for each eigenvalue and diagonal entry from both sides of Eq. (1) when $k = d$, followed by multiplying them by their respective eigenvalues and diagonal entries. We extend this reasoning to partial sums, the partial relative entropy of coherence, $C_{r\ partial}^k(\rho) = S^k(\rho_{diag}) - S^k(\rho)$ for $k < d$, isolates the coherence contribution, where S^k is the entropy restricted to the k eigenvalues or diagonal elements. These coherence measures reflect the off-diagonal quantum coherence encoded in the difference between the spectral and diagonal distributions of ρ , rooted in the structural constraints imposed by the SH majorization theorem.

We further this argument to the relative cross entropy of coherence $C_{r\ cross}(\rho)$, which captures the asymmetry between two distributions, we define

$$C_{r\ cross}(\rho) = S(\rho_{diag}||\rho) - S(\rho||\rho_{diag}), \quad (02)$$

where $S(\rho_{diag}||\rho) = -\text{Tr}(\rho_{diag} \log(\rho))$ and $S(\rho||\rho_{diag}) = -\text{Tr}(\rho \log(\rho_{diag}))$. This quantifier measures the difference in cross entropy contributions before and after decoherence, which captures how the diagonal elements fail to reconstruct the off-diagonal quantum coherence. By majorization, $\rho \succcurlyeq \rho_{diag}$, which ensures that $S(\rho_{diag}||\rho) \geq S(\rho||\rho_{diag})$, thus it guarantees the positivity of $C_{r\ cross}$. Since, ρ_{diag} does not rely on any quantum superpositions, there is less room for ρ_{diag} to move in cross-entropy space or in SH majorization relation. By contrast, ρ 's coherence structure is more susceptible to transformation under IO, and its cross-entropy $S(\rho_{diag}||\rho)$ can drop more readily. This asymmetry in how respond to an incoherent map explains why $S(\rho||\rho_{diag})$ decreases less than $S(\rho_{diag}||\rho)$ does. We

numerically demonstrated this asymmetry before and after incoherent operations, which confirm that the former decreases less than later for monotonicity (Fig. 1(a)) and strong monotonicity (Fig. 1(b)). Additionally, we have confirmed numerically that $C_{r_{cross}}$ satisfies all the resource theoretic axioms (C1-C6) for a coherence measure [8] by calculating it for 1 million quantum states with varying dimensions and number of Kraus operators. Furthermore, partial majorization relationships allow the extension to a partial relative cross entropy of coherence $C_{r_{cross}}^k(\rho) = S_{cross}^k(\rho_{diag}) - S_{cross}^k(\rho)$ where the entropies are restricted to the k eigenvalues or diagonal elements. The SH majorization ensures that the partial sums of eigenvalues and diagonal elements preserve their ordering, which provides a rigorous foundation for these coherence measures. This structural hierarchy, combined with the asymmetry introduced by cross entropy, allows $C_{r_{cross}}^k(\rho)$ and $C_{r_{cross}}(\rho)$ to serve as appropriate quantifiers of quantum coherence. Direct numerical results suggests that $C_{r_{cross}}(\rho) \geq C_r(\rho)$. While the $C_r(\rho)$ is simpler and directly tied to the von Neumann entropy difference, $C_{r_{cross}}(\rho)$ provides a more refined, asymmetric, and operationally meaningful measure of coherence, especially for high-dimensional or noisy systems, and tasks which may require detailed coherence analysis.



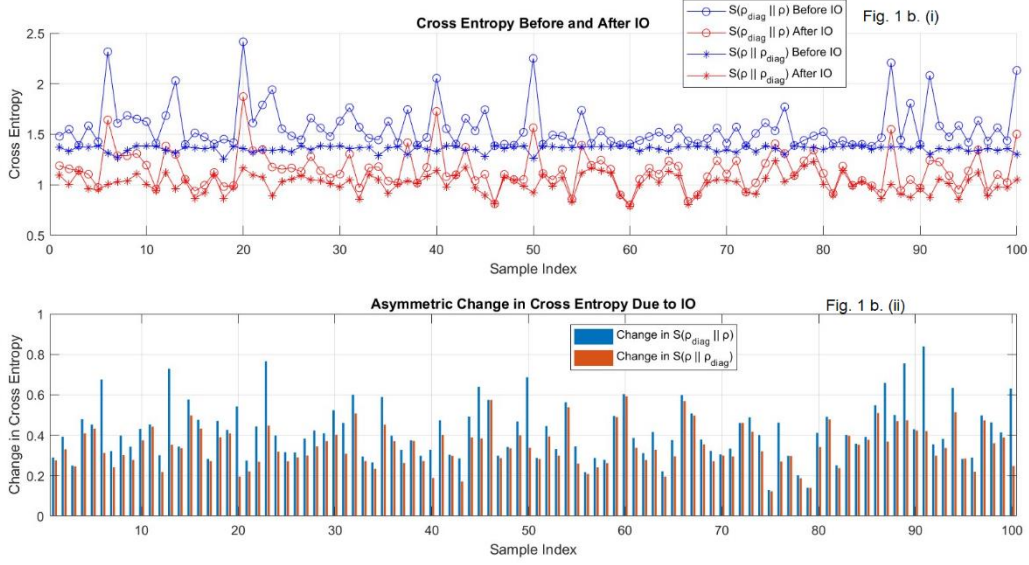


FIG. 1 (a-b) demonstrate the monotonicity and strong monotonicity effects of IO on $S(\rho_{diag} || \rho)$ and $S(\rho || \rho_{diag})$ for randomly generated density matrices. The first subplots (i) and (ii) and show highlight the asymmetry in the evolution and the changes in cross entropies, respectively, which emphasize the differential impact of IO on these measures.

Another avenue for deriving Schur–Horn (SH) majorization constraints involves using indices of polarimetric purity (the so-called Gil indices) from optical polarization theory [20–22]. By formulating these indices in terms of the eigenvalues $\{\lambda_i\}$ of a density matrix and its minimum eigenvalue λ_{min} , one obtains a majorization-like relation,

$$\sum_{i=1}^k G_j^{diag\downarrow} \geq \sum_{j=1}^k G_i^\downarrow, \quad \forall k, \quad (03)$$

where

$$G_j = \sum_{i=1}^{d-1} \lambda_i - j\lambda_{min}, \quad (04)$$

with each $G_j \leq G_{j+1}$ and $G_j \in [0,1]$; and $G_j^{diag\downarrow}$ and G_i^\downarrow denote the corresponding indices arranged in descending order. This polarization theory-inspired perspective suggests a majorization relation for polarization itself, thereby unifying aspects of quantum coherence and classical optical polarization. Moreover, by taking normalized indices, one can construct new entropy-based coherence measures directly from these relations. Overall, this bridging of quantum and classical frameworks holds promise

for novel mathematical and physical investigations into both quantum coherence and polarization properties.

Although the squared version of the SH majorization is not explicitly discussed in the general literature, we have observed that for density matrices, the squaring operation does not violate the majorization condition. We used a Monte Carlo framework to test the squared SH majorization condition on random density matrices generated using Haar-random unitary matrices, Schmidt decomposition, and eigenvalue-based constructions. Small perturbations were applied to ensure robustness while maintaining Hermiticity, positivity, and trace-1 properties. Across all tests, involving comparisons of squared eigenvalues and diagonal elements, no violations were observed, which confirms the numerical validity of the squared majorization condition. While the conjecture on the squared version of the SH majorization remains to be formally established, our findings suggest its validity in the context of density matrices. As a consequence, this opens up the possibility of deriving coherence monotones. Specifically, using the squared SH majorization, we can obtain both the partial and full relative Renyi and Tsallis of coherence for $q = 2$, which are defined as distinguishability measures $D_q(\rho || \rho_{diag})$, that may not exhibit strong monotonicity under incoherent operations [4,23]. The squared eigenvalue structure is tied closely to purity such as in the trade-off coherence-purity relation [23]. Consequently, universal bounds between the von Neumann entropy and the Tsallis-2 (since Renyi-2 \geq Tsallis-2, we chose Tsallis-2) functionals can be derived, which may reflect the interplay of spectral spread and coherence in a quantum state. These bounds provide a systematic way to characterize coherence and, therefore, offer a more geometric understanding of coherence which we describe in the next section as coherence space.

4. The Coherence Space: coherence distillation curves

We begin by considering the set of valid eigenvalue vectors $\{\lambda_i\}_{i=1}^d$ of d – dimensional density matrix ρ . Mathematically, these vectors lie in the standard probability simplex $\Delta^{d-1} \subset \mathbb{R}^d$, defined by $\lambda_i \geq 0$ and $\sum_{i=1}^d \lambda_i = 1$. Although Δ^{d-1} is itself a convex polytope with flat boundaries, we do not retain

that characterization once we map each $\{\lambda_i\}$ to the two functionals von Neuman entropy S_{vN} and Tsallis-2 entropy S_2 , which belong to the one side of the SH majorizations when $k = d$, because the transformation $\lambda \mapsto (S_2, S_{vN})$ is not linear. Consequently, the image of Δ^{d-1} in \mathbb{R}^2 becomes a curved region rather than a simplex. Moreover, by imposing additional constraints on the eigenvalue distribution (see Table. 1), we restrict ourselves to submanifolds of Δ^{d-1} , which emerge as points, boundary arcs or distinct clusters in the $S_2 - S_{vN}$ plane. Physically, S_2 rises as the eigenvalues become more uniform, which vanishes for a pure state and reaches $1 - 1/d$ for the maximally mixed state, while S_{vN} increases from 0 to $\log(d)$. Collecting all sampled points thus reveals how specific eigenvalue pattern carve out recognizable quantum state as shown in Fig. 2.

Table 1. Classification of Coherence distillation curves with eigenvalue constraints, normalization, and maximum rank. Table shows the five families of curves in a d -dimensional $S_2 - S_{vN}$, each defined by distinct eigenvalue ordering and normalization conditions. These curves serve as boundaries or special arcs in coherence analyses of quantum states. Note that middle-intermediate curves become upper degenerate curves for the sub-Hilbert space.

Coherence distillation Curve	Order constraint	Normalization Equation	maximum Rank
Lower-curve qubit states	$\{\lambda_i\}_{i=1}^2 = \lambda_e \geq \{\lambda_j\}_{j=3}^d = \lambda_0 = 0$	$\sum_{i=1}^2 \lambda_i = 1$	2
Lower-Intermediate m -curves	$\{\lambda_i\}_{i=1}^{m+1} = \lambda_e \geq \lambda_{m+2} \geq \{\lambda_j\}_{j=m+3}^d = \lambda_0 = 0$, with $m = d - 3$ for $d \geq 4$	$\sum_{i=1}^{d-2} \lambda_i + \lambda_{d-1} = 1$	$d - 1$ or $m + 2$
Lower-Upper curve	$\{\lambda_i\}_{i=1}^{d-1} = \lambda_e \geq \lambda_d \geq 0$	$\sum_{i=1}^{d-1} \lambda_i + \lambda_d = 1$	d
Middle-Intermediate n -curves	$\lambda_1 \geq \{\lambda_i\}_{i=2}^{n+2} = \lambda_e \geq \{\lambda_j\}_{j=n+3}^d = \lambda_0 = 0$, with $n = d - 3$ for $d \geq 4$	$\sum_{i=1}^{d-2} \lambda_i + \lambda_{d-1} = 1$	$d - 1$ or $n + 2$
Upper degenerate curve	$\lambda_1 \geq \{\lambda_i\}_{i=1}^d = \lambda_e \geq 0$	$\lambda_1 + \sum_{i=2}^d \lambda_i = 1$	d

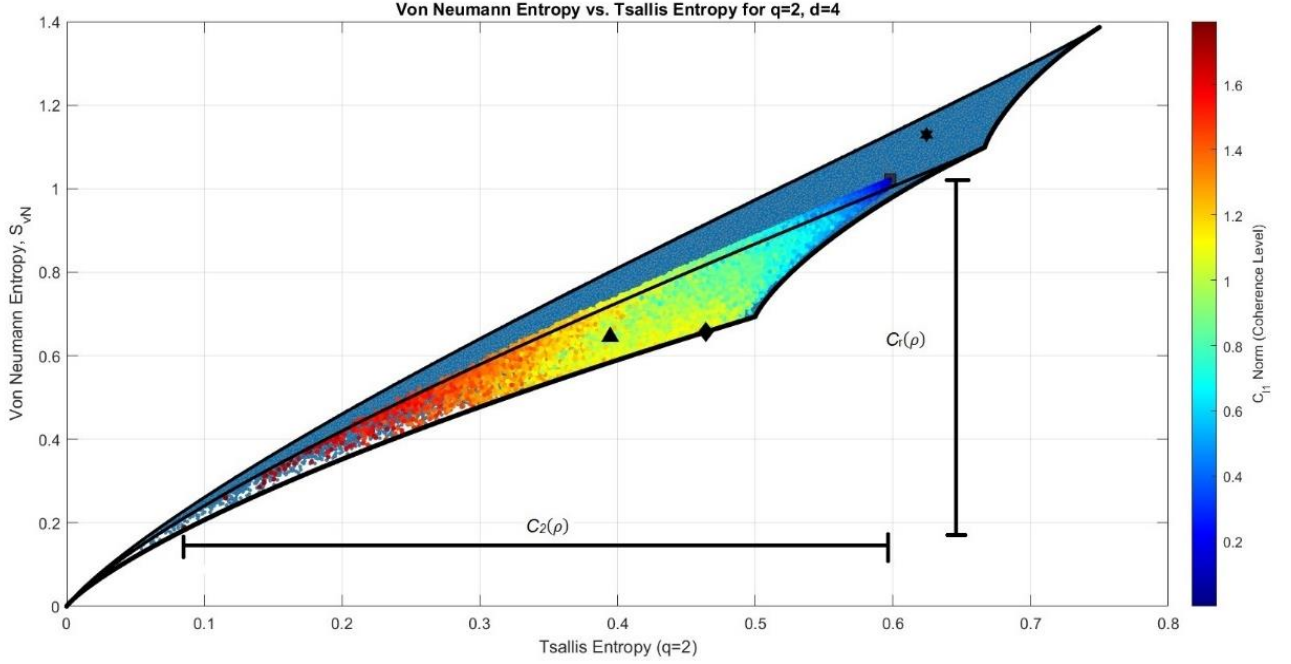


FIG. 2 illustrates $S_2 - S_{vN}$ plane for $d = 4$ density matrices of varying ranks. The horizontal and vertical lines outside the region indicates the maximum $C_r(\rho)$ and $C_2(\rho)$ for a randomly generated matrix shown with a square marker whose transitions across quantum states is shown with color map representing coherence $C_{l_1}(\rho)$. The full-rank matrix (rank 4) is marked with black hexagons, rank 3 with black triangles, and rank 2 with black diamonds, indicating sub-Hilbert spaces. Boundary curves are specified for the coherence distillation such as first-lower and upper curves belong to qubit and degenerate distillations, respectively.

The dynamics of a quantum system transitioning from a randomly mixed state as shown by a squared marker in Fig. 2 to state with increasing coherence represented by the evolution of the density matrix. We gradually introduce coherence by adding small random off-diagonal elements, with their strength increasing iteratively. By calculating $C_{l_1}(\rho)$ directly from the generated density matrices and accessing $C_2(\rho)$ and $C_r(\rho)$ from S_2 and S_{vN} , respectively, we trace the evolution of quantum states as they transition from a randomly mixed state to states with increasing coherence. By utilizing $C_{l_1}(\rho)$, we can track the evolution of coherence in quantum systems and probe specific regions of the $S_2 - S_{vN}$ plane without directly calculating the entropies at every step, which can be prohibitively expensive for large quantum systems due to the need to process the entire eigenvalue spectrum. This allows for an

efficient characterization of coherence within the coherence space, where regions of the $S_2 - S_{vN}$ plane can be explored based on $C_{l_1}(\rho)$, which reflects coherence in a more computationally tractable manner. Thus, we establish a robust framework for characterizing coherence across diverse state configurations, which may provide deeper insights into the role of coherence in quantum state evolution. This approach provides a detailed exploration of how coherence affects key information-theoretic measures, which shed light on the gradual restoration of coherence in quantum systems and its influence on their purity and entropy properties.

In Fig. 2, the lower curve delineates the boundary for qubit states on which points belong to the qubit coherence distillation. States on this curve are characterized by eigenvalue distributions $\lambda_1 \geq \lambda_2 \geq \lambda_3 = \lambda_4 = 0$, hence form a rank-2 density operator. Detailed eigenvalue distributions for any d -dimensional Hilbert space, which characterize different coherence distillation curves are given in Table 1 and shown in Fig. 3 for $d = 4$. The distillable coherence in the asymptotic limit,

$$C_d(\rho) = S(\rho^{diag}) - S(\rho), \quad (05)$$

quantifies the maximal rate at which copies of ρ can be converted to the qubit state via IO as $n \rightarrow \infty$ [24-25]. The curve indicates that concentrating all the coherence into two nonzero eigenvalues reduces the $S_{vN}(\rho)$ for a given $S_2(\rho)$, thus marking the minimal-coherence boundary wherein a significant fraction of λ_1 and λ_2 contributes directly to qubit-like coherence.

By contrast, the upper curve in Fig. 2 introduces degenerate coherence distillation, governed by the constraint $\lambda_1 \geq \lambda_2 = \lambda_3 = \lambda_4$. Such states distribute the eigenvalue weights more symmetrically, resulting in a larger $S_{vN}(\rho)$ for a specific value of $S_2(\rho)$ with the full range. We define the degenerate distillable coherence of ρ as the supremum of all achievable rates R at which ρ_{deg} can be asymptotically obtained per copy of ρ . Concretely, we say that R is achievable if there exists a sequence of free operations $\{\Delta_i\}$ such that, for sufficiently large n , the transformed state $\Delta_i[\rho^{\otimes n}]$ approximates $\rho_{deg}^{\otimes [nR]}$ with arbitrarily small error in the trace norm. Formally:

$$\lim_{n \rightarrow \infty} \text{Inf}_{\Delta_i} \|\Delta_i[\rho^{\otimes n}] - (\rho_{deg}^{\otimes [nR]})\|_1 = 0, \quad (06)$$

where $[nR]$ denotes the integer part of nR . The degenerate distillable coherence $C_d^{deg}(\rho)$ is then given by the supremum of such R over all possible free operations $\{\Delta_i\}$, such that

$$C_d^{deg}(\rho) = \sup \left\{ R \mid \lim_{n \rightarrow \infty} \text{Inf}_{\Delta_i} \|\Delta_i[\rho^{\otimes n}] - (\rho_{deg}^{\otimes [nR]})\|_1 = 0 \right\} \quad (07)$$

Here, $\rho^{\otimes n}$ represents n copies of the original state ρ , while $\rho_{deg}^{\otimes [nR]}$ is the tensor product of $[nR]$ copies of the target degenerate resource state. The condition that the trace-norm distance goes to zero ensures that, in the limit of infinitely many copies, $\rho^{\otimes n}$ can be faithfully converted into $\rho_{deg}^{\otimes [nR]}$. This mirrors the standard structure of resource theories (e.g., entanglement or coherence distillation), where a similar limit-based definition governs the optimal asymptotic rate of generating a target resource. However, the key novelty here lies in choosing ρ_{deg} with degenerate eigenvalues, rather than a single-qubit maximally coherent state. This choice enables higher-dimensional or symmetrically weighted superpositions to be distilled.

From an operational standpoint, the framework of degenerate coherence distillation can provide more efficient strategies whenever the goal is to produce states with uniform or partially uniform eigenvalue distributions. In settings such as high-dimensional quantum information tasks, the degenerate distillable coherence can significantly exceed what is possible with conventional qubit-based protocols. Essentially, symmetrical (or partially symmetrical) eigenvalues lower the overhead needed to transform multiple copies of ρ into equally weighted superpositions. This degenerate limit thus occupies the maximal-coherence boundary in the $S_2 - S_{vN}$ plane, which may indicate that for the states with partially or fully degenerate eigenvalues, the resource theory of coherence can exploit their uniform structure to achieve higher asymptotic rate of coherent-state generation than is feasible with the sharply peaked spectra underlying qubit distillation.

These insights highlight a new paradigm: rather than funneling coherence into the two dominant eigenvalues, the process on the upper curve exploits the uniformity of the eigenvalue distribution to produce symmetry-preserving coherent states. In doing so, it broadens the operational framework of coherence distillation, which may offer a more tailored and efficient approach for states with partially degenerate spectra. Although Fig. 2 is depicted for $d = 4$, the analysis provided here applies to any finite d – dimensional quantum state.

Finally, we extend beyond the usual depiction of eigenvalue distributions in the $S_2 - S_{vN}$ plane and move into the $S_{vN} - (1 - \lambda_{max})$ plane. As detailed below, this new perspective reveals a refined, state-dependent entropic uncertainty relation that surpasses standard bounds. Of course, this parameter space can also yield broader insights into the resource-theoretic properties of quantum coherence. Nevertheless, we now focus on deriving and analyzing a novel entropic uncertainty relation, one that explicitly incorporates the largest eigenvalue of a state to tighten uncertainty constraints beyond existing limits.

5. Refined Entropic Uncertainty via Maximum Eigenvalues:

To illustrate the main idea, let us consider any d -dimensional quantum state ρ . Numerical evidence (see Fig. 3) shows that its von Neumann entropy $S_{vN}(\rho)$ consistently exceeds quantity $1 - a$, where $a = \lambda_{max}(\rho)$ is the largest eigenvalue of ρ . For simplicity, we assign the remaining $d - 1$ eigenvalues each to $\frac{1-a}{d-1}$. Introducing the notation $x \equiv S_{vN}(\rho)$ and $y \equiv 1 - a$, we treat a as a parameter spanning $\left[\frac{1}{d}, 1\right]$. This gives

$$x(a) = -\left[a \log a + (1 - a) \log \left(\frac{1-a}{d-1}\right)\right], \quad (08)$$

and

$$y(a) = 1 - a. \quad (09)$$

A direct derivative calculation shows that $x(a)$ is strictly decreasing in a , whereas $y(a)$ is also decreasing in a . Eliminating a thus renders y as an increasing function $y(x)$. Further, since the second derivative

$x''(a) < 0$, the map $a \mapsto x(a)$ is strictly concave in a , which implies $x \mapsto y(x)$ is strictly convex. Hence $\{(x(a), y(a))\}$ sweeps out a smooth, monotonically increasing boundary curve in the $(S_{vN}, 1 - \lambda_{max})$ plane (see Fig. (3)). This curve runs from a $(0,0)$ at $a = 1$ to $(\log d, 1 - 1/d)$ at $a = 1/d$. Similar arguments hold for the upper curves bounding the plane from above, hence, upper and lower bounds these curves can readily be defined. Furthermore, the reference blue line in Fig. 3 shows that any point located on the plane satisfies, $S_{vN} > 1 - \lambda_{max}$. Therefore, the boundary curves in the in the $(S_{vN}, 1 - \lambda_{max})$ plane for eigenvalues distribution,

$$S_{vN}(\rho) \geq 1 - \lambda_{max}(\rho), \forall \rho, \quad (10)$$

thereby reveals a fundamental, state-dependent constraint between entropy and λ_{max} .

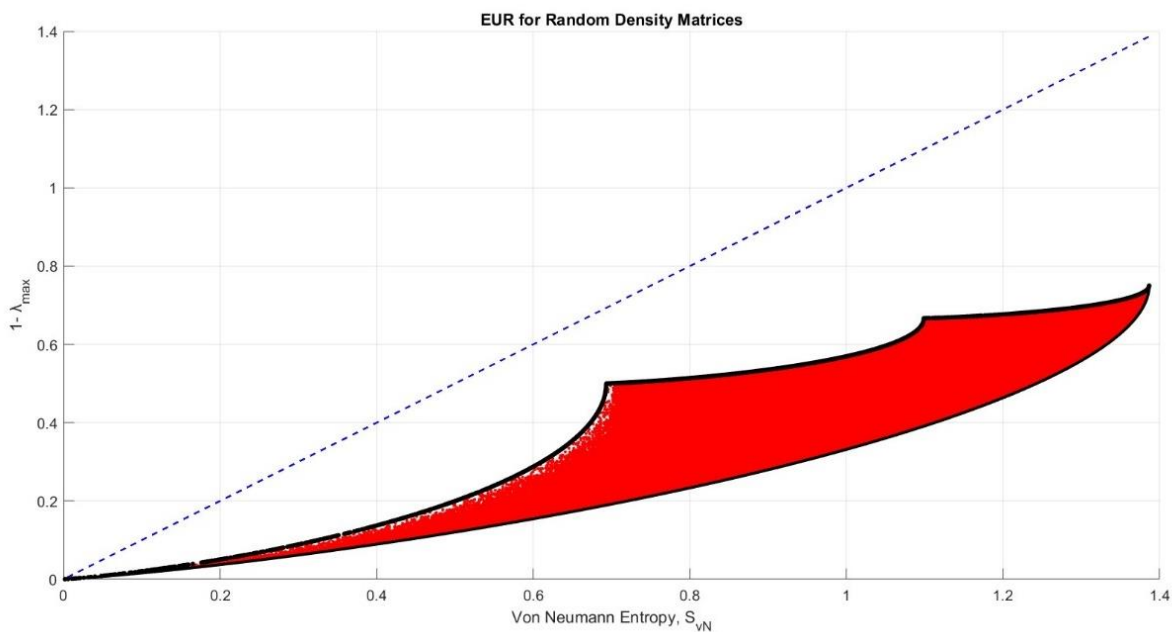


FIG. 3 explores the relationship between von Neumann entropy S_{vN} and $\sum_{i=2}^d \lambda_i = 1 - \lambda_{max}$ for randomly generated density matrices. Data points represent matrices with varying eigenvalue distributions, and a reference line $y = x$ indicates equality which is always above the bound for any dimension and shown here for $d = 4$.

Building on this, we extend the framework to measurement outcomes. Define $\lambda_{max}^j(\rho)$, $j = X, Z$ as the largest eigenvalue of the post-measurement state in basis j (for instance, $j = X$ or $j = Z$). Substituting the corresponding Shannon entropies $H(j, \rho)$, for $S_{vN}(\rho)$, one obtains

$$H(X, \rho) + H(Z, \rho) \geq 2 - [\lambda_{max}^X(\rho) + \lambda_{max}^Z(\rho)]. \quad (11)$$

Indeed, this can be extended to N number of measurement bases. In contrast to standard Massen-Uffink (MU) uncertainty bound [24], which depends on only the overlap of the two bases, this state-dependent relation tightens whenever $\lambda_{max}^j(\rho)$ is sufficiently small, or one can take n root values of $1 - \lambda_{max}^j(\rho)$ to make the bound further tightened, and hence, one can obtain the tightest possible bound. Therefore, Eq. (11) is more refined quantum-information constraint. Thus, replacing the overlap term c in MU by a combination of $1 - \lambda_{max}(X) + 1 - \lambda_{max}(Z)$ yields an operational entropic bound that is sensitive to the actual state ρ under consideration, rather than merely the geometry of the two measurement bases.

This state-sensitive perspective on entropic uncertainty is novel in that it unifies spectral properties of ρ with measurement-based entropies, which offers a sharper look into fundamental quantum limits. It can be extended to any number N of observables, which paves the way for enhanced uncertainty relations in multi-basis scenarios—a direction previously hampered by less adaptive bounds. This stands in contrast to earlier approaches that could not exploit such state-dependent information and thus remained looser in many physically relevant regimes. As a result, our refined EUR not only provides deeper insight into the interplay between measurement outcomes and the underlying spectral structure of quantum states, but also offers a versatile and experimentally relevant tool. It has potential applications spanning quantum metrology, cryptography, and the general resource theories of coherence and entanglement, where tighter entropic bounds translate directly into more precise or more secure protocols. By highlighting how $\lambda_{max}(J)$ influences fundamental uncertainty, we establish an operationally meaningful route to customizing quantum-information constraints in real-world settings, which may promise both conceptual advances and practical benefits for the research in quantum science.

6. Conclusion:

We have introduced a rigorous framework underpinned by the Schur–Horn (SH) majorization theorem to quantify and visualize quantum coherence in d -dimensional systems. By analyzing how eigenvalues and diagonal elements of density matrices relate, we derived both standard and partial forms of the relative entropy of coherence and relative cross-entropy of coherence, as well as associated entropy–coherence monotones. These measures yield a unified toolkit for tracking coherence in physically realizable states and for delineating precise coherence-distillation boundaries within the von Neumann–Tsallis entropy diagrams.

A key insight is the concept of degenerate coherence distillation, whereby the symmetry of the eigenvalue spectrum can lead to enhanced coherence extraction. This finding broadens the operational landscape beyond the traditional qubit-centric paradigm, which suggests that high-dimensional or partially degenerate states can be harnessed more effectively. Additionally, we proposed a refined entropic uncertainty relation that incorporates the interplay between entropy and the largest eigenvalue to yield state-dependent, and thus tighter, uncertainty constraints.

Collectively, our results underscore the flexibility and power of the SH majorization approach for studying quantum coherence. By merging geometric and operational perspectives, we offer both fundamental insights into coherence as a quantum resource and practical tools that can advance quantum information processing.

7. Acknowledgement:

This work was supported by the National Natural Science Foundation of China (Grant Nos. 12475009, 12075001, and 61601002), Anhui Provincial Key Research and Development Plan (Grant No. 2022b13020004), Anhui Province Science and Technology Innovation Project (Grant No. 202423r06050004), and Anhui Provincial University Scientific Research Major Project (Grant No. 2024AH040008).

8. References:

1. R. J. Glauber, Coherent and incoherent states of the radiation field, *Phys. Rev.* **131**, 2766 (1963).
2. E. C. G. Sudarshan, Equivalence of semiclassical and quantum mechanical descriptions of statistical light beams, *Phys. Rev. Lett.* **10**, 277 (1963).
3. E. Wolf, *Introduction to the Theory of Coherence and Polarization of Light* (Cambridge University Press, Cambridge, 2007).
4. T. Baumgratz, M. Cramer, and M. B. Plenio, Quantifying coherence, *Phys. Rev. Lett.* **113**, 140401 (2014).
5. F. Levi and F. Mintert, A quantitative theory of coherent delocalization, *New J. Phys.* **16**, 033007 (2014).
6. E. Chitambar and G. Gour, Comparison of incoherent operations and measures of coherence, *Phys. Rev. A* **94**, 052336 (2016).
7. E. Chitambar and G. Gour, Critical examination of incoherent operations and a physically consistent resource theory of quantum coherence., *Phys. Rev. Lett.* **117**, 030401 (2016).
8. Streltsov, G. Adesso, and M. B. Plenio, Colloquium: Quantum coherence as a resource., *Rev. Mod. Phys.* **89**, 041003 (2017).
9. S. Du, Z. Bai, and Y. Guo, Conditions for coherence transformations under incoherent operations., *Phys. Rev. A* **91**, 052120 (2015).
10. H. Zhu, Z. Ma, Z. Cao, S. M. Fei, and V. Vedral, Operational one-to-one mapping between coherence and entanglement measures, *Phys. Rev. A* **96**, 032316 (2017).
11. P. Harremoës and F. Topsøe, Inequalities between entropy and index of coincidence derived from information diagrams, *IEEE Trans. Inf. Theory* **47**, 2944 (2001).
12. P. Harremoës and F. Topsøe, Information diagrams: entropy, index of coincidence and probability of error, in *IEEE International Symposium on Information Theory* (2001).
13. Aiello and J. P. Woerdman, Physical bounds to the entropy-depolarization relation in random light scattering., *Phys. Rev. Lett.* **94**, 090406 (2005).
14. Tariq, P. Li, D. Chen, D. Lv, and H. Ma, Physically realizable space for the purity-depolarization plane for polarized light scattering media, *Phys. Rev. Lett.* **119**, 033202 (2017).
15. E. Rastegin, Uncertainty relations in terms of generalized entropies derived from information diagrams, *arXiv:2305.18005* (2023).
16. S. Huang, H. L. Yin, Z. B. Chen, and S. Wu, Entropic uncertainty relations for multiple measurements assigned with biased weights, *Phys. Rev. Res.* **6**, 013127 (2024).

17. M. Atiyah, Convexity and commuting Hamiltonians, *Bull. Lond. Math. Soc.* **14**, 1 (1982).
18. J. Hilgert, K. H. Neeb, and W. Plank, Symplectic convexity theorems, *Sem. Sophus Lie* **3**, 123 (1993).
19. M. A. Nielsen, Lecture Notes, Department of Physics, University of Queensland, Australia (2002).
20. J. J. Gil, Polarimetric characterization of light and media: physical quantities involved in polarimetric phenomena, *Eur. Phys. J. Appl. Phys.* **40**, 1 (2007).
21. San José and J. J. Gil, Invariant indices of polarimetric purity: generalized indices of purity for $n \times n$ covariance matrices., *Opt. Commun.* **284**, 38 (2011).
22. J. Gil, A. Norrman, A. T. Friberg, and T. Setälä, Polarimetric purity and the concept of degree of polarization., *Phys. Rev. A* **97**, 023838 (2018).
23. E. Rastegin, Quantum-coherence quantifiers based on the Tsallis relative α entropies, *Phys. Rev. A* **93**, 032136 (2016).
24. X. Yuan, H. Zhou, Z. Cao, and X. Ma, Intrinsic randomness as a measure of quantum coherence, *Phys. Rev. A* **92**, 022124 (2015).
25. Winter and D. Yang, Operational resource theory of coherence., *Phys. Rev. Lett.* **116**, 120404 (2016).
26. H. Maassen and J. B. Uffink, Generalized entropic uncertainty relations, *Phys. Rev. Lett.* **60**, 1103 (1988).